Available online at www.sciencedirect.com
SCIENCE DIRECT
Polymer 47 (2006) 4985–4995
polymer
www.elsevier.com/locate/polymer

'Nano-tree'—type spherical polymer brush particles as templates for metallic nanoparticles

Yan Lu [a,*], Yu Mei [a], Roland Walker [a], Matthias Ballauff [a,*], Markus Drechsler [b]

[a] *Physikalische Chemie I, University of Bayreuth, 95440 Bayreuth, Germany*
[b] *Makromolekulare Chemie II, University of Bayreuth, 95440 Bayreuth, Germany*

Received 3 April 2006; received in revised form 10 May 2006; accepted 11 May 2006
Available online 2 June 2006

Abstract

We present a new type of spherical polymer brush particles that consist of a solid poly(styrene) core (diameter: ca. 100 nm) onto which chains of a bottlebrush polymer have been densely grafted. These systems were prepared in aqueous dispersion by photo emulsion-polymerization using the macromonomer poly(ethylene glycol) methacrylate (PEGMA). In opposite to conventional spherical polyelectrolyte brushes carrying linear polymer chains, the system prepared here has a shell consisting of regularly branched chains ('nano-tree'-type morphology). The branches consist of oligo(ethylene glycol) chains ($n=13$) terminated by a hydroxyl group. We demonstrate that these particles can be used as nanoreactors for the generation and immobilization of well-defined silver nanoparticles. Cryo-TEM and FESEM images show that Ag nanoparticles with diameter of $\sim 7.5 \pm 2$ nm are homogeneously embedded into the PS–PEGMA brushes. Moreover, the composite particles exhibit an excellent colloidal stability. The catalytic activity is investigated by monitoring the reduction of 4-nitrophenol by $NaBH_4$ in presence of these silver nano-composite particles. The rate constant k_{app} was found to be strictly proportional to the total surface of the nanoparticles in the system. The study of the temperature dependence shows that the rate constants k_{app} obtained at different temperatures leads to an activation energy of 62 kJ/mol.

Keywords: Polymer brush; Silver nanoparticles; Nanoreactor

1. Introduction

Nanoparticles consisting of noble metals have recently attracted much attention because such particles may exhibit properties differing strongly from the properties of the bulk metal [1]. Thus, such nanoparticles have interesting perspectives in the applications as catalysts [1–5], sensors [6], and electronics. However, the metallic nanoparticles must be stabilized in solution in order to prevent aggregation. Application in catalysis hence requires immobilization in suitable carrier systems such as dendrimers [7–9], latex particles [10–14], microgels [15–22], or other polymers [23,24]. In principle, suitable carrier systems may be used as a 'nanoreactor', in which the metal nanoparticles can be immobilized and used for the purpose at hand. Thus, Crook's group [25,26] reported that dendrimers can act as both templates and porous nanoreactors and the dendrimer-encapsulated noble metal clusters show highly catalytic activity.

Recently, spherical polyelectrolyte brushes have been introduced as carrier system of metal nanoparticles [27,28]. These systems consist of a solid poly(styrene) core onto which long anionic or cationic polyelectrolyte chains are densely grafted. The use of the cationic spherical polyelectrolyte brushes as nanoreactors has a number of clear advantages. The surface of nearly monodisperse core particles is well defined and approximately 95% of the counter-ions are confined in the brush layer [29]. Hence, metal ions can be confined as counterions within the brush layer. Subsequent reduction of the metal salt within the 'nanoreactors' thus defined leads to gold, platinum or palladium nanoparticles [27,28]. For these metals well-defined particles with narrow size distribution have been obtained. However, using the spherical polyelectrolyte for the generation of silver nanoparticles leads to unsatisfactory results. We found that the Ag-nanoparticles partially coagulate to form much larger particles that exhibit a broad size distribution. Obviously, the nanoparticles formed at first possess enough diffusional mobility and their immobilization within a conventional spherical brush is not sufficient.

* Corresponding authors. Tel.: +49 921 55 2760; fax: +49 921 55 2780.
E-mail addresses: yan.lu@uni-bayreuth.de (Y. Lu), matthias.ballauff@uni-bayreuth.de (M. Ballauff).

0032-3861/$ - see front matter © 2006 Elsevier Ltd. All rights reserved.
doi:10.1016/j.polymer.2006.05.027

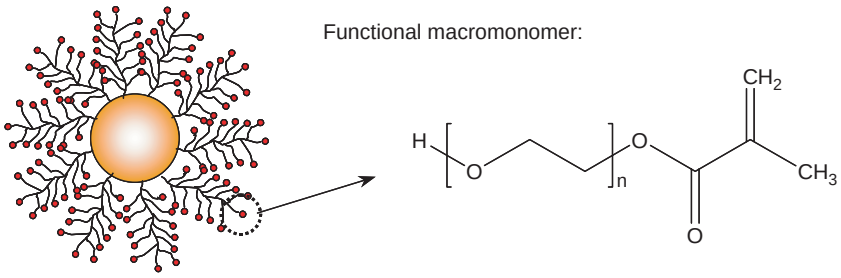

Fig. 1. Model for the 'nano-tree' type PS–PEGMA brushes prepared by the macromonomer of hydroxy poly(ethylene glycol) methacrylate (PEGMA) ($n=13$).

In this paper, we describe a new type of colloidal spherical polymer brush system synthesized by photo-emulsionpolymerization of the macromonomer poly(ethylene glycol) methacrylate (PEGMA). Using this method, the bottlebrush chains are affixed to colloidal poly(styrene) sphere by a 'grafting from' technique [30–32]. The poly(ethylene oxide) (PEO) macromonomer has recently been used repeatedly to prepare defined comb- or star-like polymers [33,34], or as reactive stabilizer to prepare well-defined polymeric microspheres [35,36]. In the present work, the hydrophilic ω-hydroxy PEO macromonomer is used as the monomer for photo-polymerization. Fig. 1 shows the structure of these particles in a schematic fashion: the surface of colloidal core particles is covered by highly branched polymer chains. Hence, a 'nano-tree'-type morphology can be achieved for the brush layer attached to the core particles. Moreover, the hydrophilic hydroxyl end groups from the macromonomer will functionalize the polymer brushes, and further modification of the polymer brush or combination of the polymer brush particles into hydrogels will become possible [37].

As shown in Fig. 2, the synthesis of these particles can be carried out in three steps: in the first step, PS core particles are prepared by a conventional emulsion polymerization [38]. In a second emulsionpolymerization, these core particles will be covered by a thin layer of the photo-initiator HMEM, which is a monomer at the same time (Fig. 2). In the third step, the photo-emulsionpolymerization is started by UV irradiation onto the suspension of these latex particles. Thus, radicals are generated on their surface, which start the radical polymerization of water-soluble macromonomer PEGMA in aqueous solution. By this grafting-from strategy highly branched polymer brushes are generated on the surface of the core particles [38].

Here, we demonstrate that these particles may be used as well-defined nanoreactors for the generation of stable Ag-nanoparticles. Cryogenic transmission electron microscopy (cryo-TEM) [39–41] is used to investigate the morphology of the resulting composite particles in situ, that is, in aqueous phase. The morphology of the Ag-composite particles obtained here is compared to the Ag nanoparticles, which were prepared by using cationic or anionic polyelectrolyte brushes as template. Moreover, the catalytic activity of silver nanocomposites has been investigated using the reduction reaction of 4-nitrophenol by sodium borohydride as a benchmark reaction [3,28,42].

2. Experimental part

2.1. Materials

Macromonomer hydroxy poly (ethylene glycol) methacrylate (PEGMA, $M_w=527$; Aldrich), sodium dodecyl sulfate (SDS; Fluka), and potassium peroxodisulfate (KPS; Fluka) were used as received. Styrene (BASF) was destabilized by Al_2O_3 column and stored in the refrigerator. 2-[*p*-(2-Hydroxy-2-methylpropiophenone)]-ethyleneglycol methacrylate (HMEM) was used as the photo-initiator. The synthesis of this compound has been described previously [38,43]. Silver nitrate ($AgNO_3$) and sodium borohydride ($NaBH_4$) (p.A.) were purchased from Aldrich and used as received. 4-Nitrophenol (p.A.) was obtained from Aldrich and used as received.

2.2. Methods

Photo-emulsion polymerization was done in a UV-reactor (Heraeus TQ 150 Z3, range of wavelengths 200–600 nm). Cryogenic transmission electron microscopy (cryo-TEM) specimens were prepared by vitrification of thin liquid films supported on a TEM copper grid (600 mesh, Science Services, Munich, Germany) in liquid ethane at its freezing point. The specimen was inserted into a cryotransfer holder (CT3500, Gatan, Munich, Germany) and transferred to a Zeiss EM922 EFTEM (Zeiss NTS GmbH, Oberkochen, Germany). Examinations were carried out at temperatures around 90 K. The TEM was operated at an acceleration voltage of 200 kV. All images were recorded digitally by a bottom-mounted CCD camera system (UltraScan 1000, Gatan, Munich, Germany) and processed with a digital imaging processing system (Digital Micrograph 3.9 for GMS 1.4, Gatan, Munich, Germany) [41].

Field-emission scanning electron microscopy (FESEM) was performed using a LEO Gemini microscope equipped with a field emission cathode. Dynamic light scattering measurements were done using an ALV 4000 light scattering goniometer (Peters) at different temperatures at a scattering angle of 90°. The UV-spectra were measured by Lambda 25 spectrometer supplied by Perkin–Elmer. The silver content was determined by thermogravimetric analysis (TGA) using a Mettler Toledo STARe system. After drying in the vacuum overnight, the silver composites were heated to 800 °C with a heating rate of 10 °C/min under N_2. The theoretical specific surface area of silver particles was estimated from these TGA results, and the

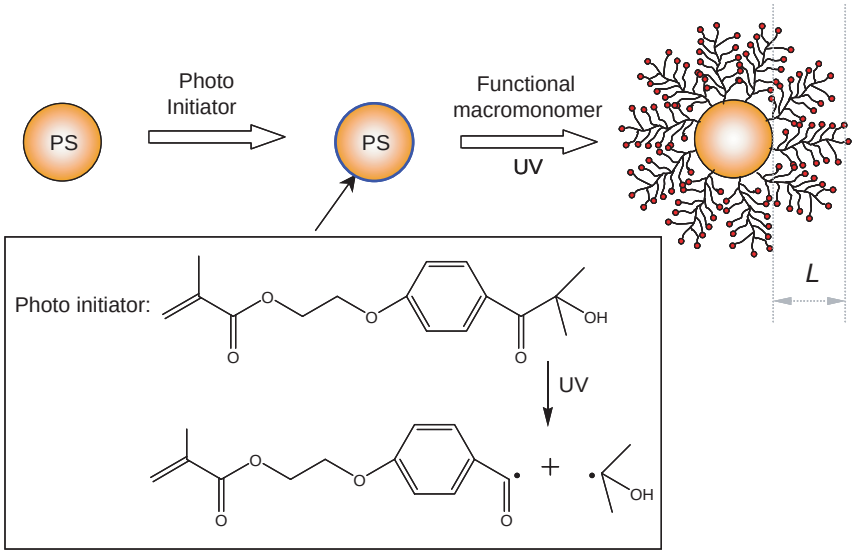

Fig. 2. Schematic representation of the preparation of PS–PEGMA brushes. In the first step, poly(styrene) (PS) core particles were prepared by a conventional emulsion polymerization. In a second step, the PS-cores were covered with a thin layer of photo-initiator HMEM. In the third step, the shell of highly branched brushes was formed by photo-emulsionpolymerization: shining light on the aqueous suspension of these particles generates radicals at their surface which initiate the radical polymerization of the macromonomer PEGMA on the surface of the core particles.

particle size was obtained from cryo-TEM. For this calculation, the density of bulk silver was used ($\rho = 10.5$ g/cm^3).

2.3. Synthesis of the 'nano-tree' type spherical polymer brushes

The 'nano-tree'-type polymer brush particles were synthesized as shown in Fig. 2. First, PS core covered with a thin layer of photo initiator was prepared by conventional emulsion polymerization. In a typical run, 2.07 g SDS was dissolved in 820 g water under stirring. Then 208 g styrene was added. The polymerization was started by adding the initiator (0.44 g KPS dissolved in 20 g water in advance) into the solution. The reaction was run at 80 °C for 1 h, and then the temperature was lowered to 70 °C. 10.64 g HMEM dissolved in 9 g acetone was added under starved conditions at 70 °C. The slow addition (0.5 ml/min) ensured that the monomer HMEM does not form new particles [38]. After the last addition, the latex was cooled down to room temperature and purified by serum replacement against the 10-fold volume of pure water.

The PS–PEGMA brush was prepared by photo-emulsion-polymerization [38]. Diluted PS core solution (2.5 wt%) was mixed with defined amount of macromonomer hydroxy poly(ethylene glycol) methacrylate (PEGMA (15 mol% with regard to the amount of styrene)) under stirring. The whole reactor was degassed by repeated evacuation and subsequent addition of nitrogen at least 5 times. Photo polymerization was done by use of UV/vis-radiation at room temperature for 1 h. Vigorous stirring ensured homogeneous conditions. To remove possible coagulum the latex was filtered over glass wool.

All pertinent parameters, namely, the core radius R and the thickness L of the attached chains as determined by dynamic light scattering are shown in Table 1.

2.4. Preparation of the silver nanocomposites

The preparation of silver nanoparticles in an aqueous solution was carried out by the chemical reduction of silver salt–polymeric brush mixture with sodium borohydride as shown in Fig. 3. For a typical experiment, 1.2 ml $AgNO_3$ (0.1 M) solution was added to 95 g diluted polymer brush aqueous solution (solid content 0.093 wt%), and the mixture was stirred for 30 min under N_2. Thereafter, sodium borohydride (0.092 g dissolved in 5 g water) was quickly added to the solution under stirring for 1 h. Thereafter, the silver nanocomposite particles were cleaned by serum replacement against purified water (membrane: cellulose nitrate with 100 nm pore size supplied by Schleicher and Schuell).

2.5. Catalytic reduction of 4-nitrophenol

0.5 ml sodium borohydride solution (60 mmol/l) was added to 2.5 ml 4-nitrophenol solution (0.12 mmol/l) contained in a

Table 1
Characterization of the spherical polymeric brushes

Label	PS core (g)[a]	PEGMA (g)	Water (g)	R_{core} (nm)[b]	L (nm)[b]	σ (nm^{-2})[c]
PS–PEGMA	305.8	14.2	460	73.4	73	ca. 0.03

[a] Solid content for PS core dispersion is 6.12 wt%.
[b] R_{core} and L are measured by DLS at 25 °C.
[c] σ is the estimated grafting density of PEGMA chains on the PS core surface.

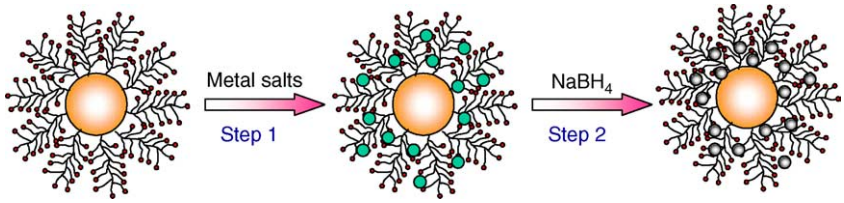

Fig. 3. Preparation of PS–PEGMA–Ag composite particles: Ag-ions are adsorbed by the brush particles in aqueous phase. Subsequent reduction leads to well-defined Ag-nanoparticles immobilized in the dense surface layer of the particles.

glass vessel. After that a given amount of the composite particles was added. Immediately after addition of composite-particles, UV spectra of the sample were taken every 30 s in the range of 250–550 nm. The rate constant of the reaction was determined by measuring the change in intensity of the peak at 400 nm with time [42].

The anionic and cationic spherical polyelectrolyte brushes used for comparison in this study have been prepared as described in Ref. [28]. Table 2 summarized the characteristic data of these particles.

3. Results and discussion

3.1. Silver nanocomposite particles

The synthesis of PS core particles by emulsion polymerization, and polyelectrolyte brushes by photo-emulsionpolymerization has been reported recently by us [27,38,43]. For anionic or cationic polyelectrolyte brushes, water-soluble monomers such as sodium styrenesulfonate (NaSS), (2-methylpropenoyloxyethyl) trimethylammonium chloride, have been used giving spherical polyelectrolyte brushes with negative or positive charge, respectively. Here, the macromonomer PEGMA was chosen to be used as the water-soluble monomer for preparation of polymer brushes. Photo-polymerization of this macromonomer was carried out as described previously [38,43]. Thus, the radicals formed by photolysis of the HMEM groups on the surface of the core particles will start the radical polymerization of shell. The formation of the brush was confirmed by the increase in particle size followed by dynamic light scattering as shown in Fig. 4. Since the radius of the PS core particles is known, DLS leads directly the thickness L of the brush layer. From Table 1, $L=73$ nm has been obtained for the PS–PEGMA brush particles when 15 mol% macromonomer was used for photo-polymerization, which indicates the formation of polymer brushes on the core surface. Moreover, the grafting density of PEGMA brush has been estimated to be of the order of 0.03 nm^{-2} (cf. also Ref. [38,43]). This demonstrates the dense grafting of the PEGMA chains on the PS cores. Fig. 5 presents the typical FESEM image and cryo-TEM image for PS–PEGMA latex particles, respectively. From the FESEM image, it can be clearly seen that practically monodisperse PS–PEGMA particles can be prepared by photo-emulsionpolymerization. Cryo-TEM image has been taken by shock-freezing the aqueous suspension of the particles. No staining of any sort was used to enhance contrast. Fig. 5(b) displays a typical cryo-TEM micrograph. The PEGMA brush affixed onto the PS cores can be seen directly on these micrographs.

The 'nano-tree'-type PS–PEGMA spherical brushes can now be used as templates for the generation and immobilization of silver nanoparticles. In order to compare the influence of polymer template on the morphology of the resulting silver composite particles, anionic and cationic polyelectrolyte brushes have also been used as the carrier systems. Fig. 6 shows the TEM images of the silver nano-composite particles, which are prepared in the presence of anionic, of cationic or of 'nano-tree' type polymer brushes, respectively. For the TEM measurements, the evaporation of water will induce the shrinkage of the spherical polymer particle partially, but will not influence the morphology of silver nanoparticles. From Fig. 6, it can be observed clearly that silver nanocomposite particles with totally different morphology are formed when different kinds of polymer brush are used as the template: when anionic spherical polyelectrolyte brushes have been used as template, monodisperse Ag nanoparticles can be found mostly in the vicinity of the polyelectrolyte brush particles. This may due to the reason that although in the initial period positive charged Ag^+ ions can be absorbed into anionic polyelectrolyte brushes. However, after the reduction of silver ions with sodium borohydride, borohydride ions will adsorb onto the surface of silver particles leading to a negatively charged surface of the Ag nanoparticles [44,45]. Thus, these Ag nanoparticles will be expelled from the anionic polyelectrolyte brushes due to the electrostatic forces as shown schematically in Fig. 7(a).

Table 2
Characterization of the spherical polyelectrolyte brushes

Label	Charge	R_{core} (nm)	L (nm)	M_w (g/mol)	L_c (nm)	L_c/R
SPB-30	Positive	46	145	150,800	182	3.96
LQ-9	Negative	58	47	49,200	60	1.03

R_{core}, core radius of polystyrene; L, thickness of the polyelectrolyte brush measured by DLS, the ionic strength in solution was 0.007 mol/L for the cationic system SPB-30 and 0.084 mol/L for the anionic system LQ-9; M_w, molecular weight of grafted chains as determined by viscosimetry; L_c, contour length of grafted chains determined by M_w.

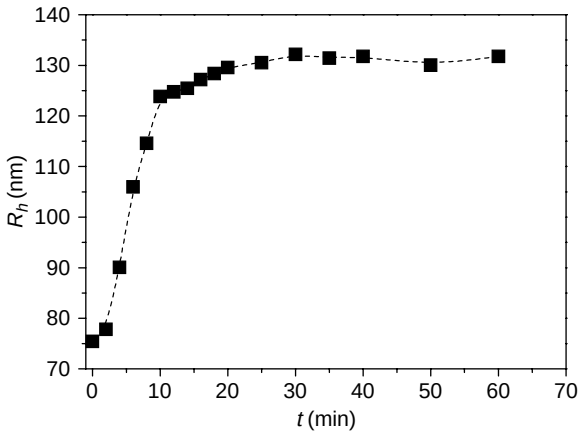

Fig. 4. Increase of the particle size of PS–PEGMA brushes with UV irradiation time measured by DLS at 25 °C.

When cationic polyelectrolyte brush has been used as the template, a different situation arises: the nucleation of silver particles will now occur in the solution as Ag^+ ions cannot be absorbed into cationic polyelectrolyte brushes. The silver nanoparticles resulting from the reduction of the silver ions will aggregate and will be stabilized only when negatively charged Ag particles are absorbed onto the cationic polyelectrolyte brush surface. This is shown schematically in Fig. 7(b). Hence, as shown in Fig. 6(b) large silver aggregates are resulting from this uncontrolled aggregation when using cationic polyelectrolyte brushes as template.

It has been reported that polar head groups, such as the hydroxyl, thiol, amine, and nitrile groups, on the surface of the polymer microspheres had a high affinity for metal nanoparticles [11,24,46,47]. Thus, when polymer brush prepared by functional macromonomer PEGMA was used as the template, the hydroxyl groups on the polymer brushes will have a high affinity for Ag^+ and silver nanoparticles. Moreover, the highly branched polymer brush will prevent the release and aggregation of the immobilized silver nanoparticles by steric hindrance and thus exert control of the growth process by diffusion control. From this point of view, this kind of 'nano-tree' type PS–PEGMA polymer brush will be a suitable carrier system for the controlled generation of silver nanoparticles. Moreover, as the PEGMA brush chains in this case are neutral, the negative charge from the obtained silver nanoparticles will not affect the stability of the composites. From Fig. 6(c) it can be seen clearly that silver nanoparticles are homogeneously embedded into the polymer brushes.

From this comparison, we can conclude that the architecture of polymer brush plays an important role in the preparation of silver nanocomposite particles. The TEM image (Fig. 6(c)) demonstrates that the 'nano-tree'-type PS–PEGMA particles are the system of choice for the generation and immobilization of well-defined silver nanoparticles.

In order to study the morphology of PS–PEGMA–Ag composite particles in situ, cryogenic transmission electron microscopy (cryo-TEM) has been employed. Fig. 8 displays the cryo-TEM images for silver nano-composites prepared by using PS–PEGMA brush as the template. In Fig. 8, dark spherical area indicates the PS cores whereas the light lines affixed on the dark core are PEGMA brushes. It is shown that silver nanoparticles are homogeneously embedded into the spherical PS–PEGMA brushes. This is also accord with the results from TGA measurement that 15.2 wt% silver has been incorporated. The analysis of the cryo-TEM images indicates that silver nanoparticles are relatively narrow dispersed with the diameter of $\sim 7.5 \pm 2$ nm. The particle size distribution histogram of Ag nanoparticles evaluated from cryo-TEM images is shown in Fig. 8(c). FESEM image made for the silver composite particles in back scattered electron (BSE) mode is shown in Fig. 9. In this case, the metal nanoparticles show up as bright dots in the dark image. From Fig. 9, small bright silver particles can be seen to be rather homogeneously distributed over the PS particle surface in accord with micrographs obtained from cryo-TEM.

After the addition of $NaBH_4$ into the system the color of the solution changed to yellow immediately, which is a

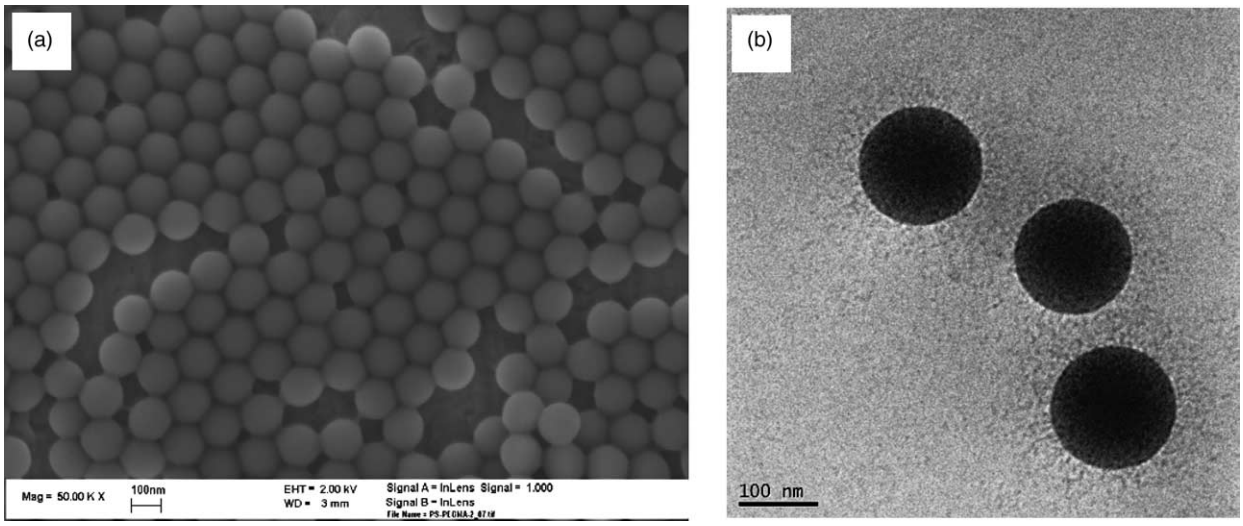

Fig. 5. FESEM image (a) and cryo-TEM image (b) of PS–PEGMA latex particles, respectively.

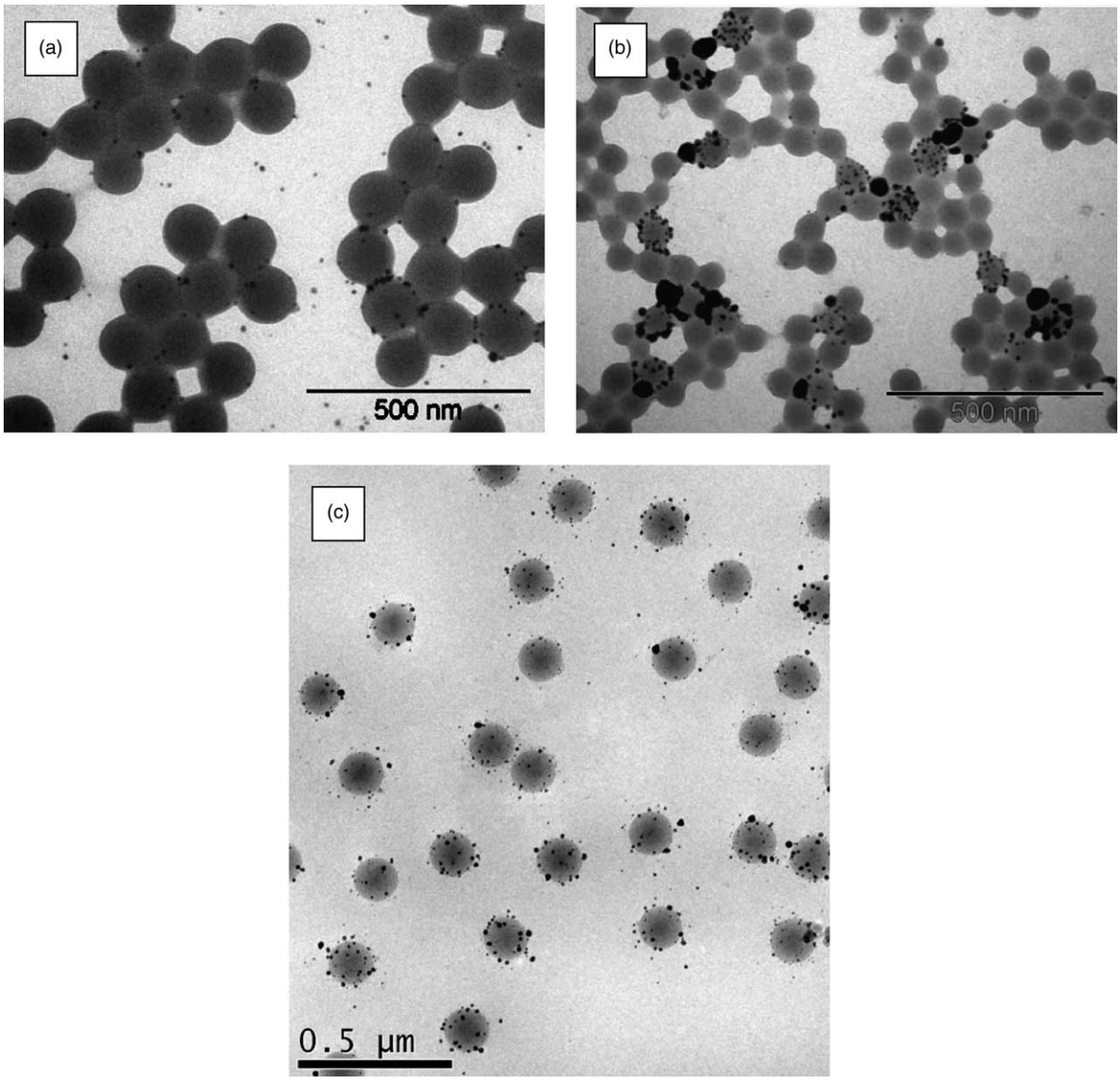

Fig. 6. TEM images for the silver nano-composite particles prepared by using anionic (a), cationic (b) polyelectrolyte brush as the template, and cryo-TEM image for the silver nano-composite particles prepared by using PS–PEGMA brush (c) as the template.

typical color for silver nanoparticles. This indicates that monodisperse silver nanoparticles are formed in the system. In order to investigate the surface plasmon absorption of the sample, UV spectra have been taken for the solution before and after reduction, which are shown in Fig. 10. From Fig. 10, it can be observed that the surface plasmon absorption band of the PS–PEGMA–Ag composites is quite sharp and a peak at 410 nm can be obtained. Similar results have been also reported by other groups [48]. Moreover, it is worth noting that the dispersion of silver composite particles is quite stable. Neither obvious sedimentation nor the shift of the maximal of the surface plasmon absorption band has been found for the purified samples after storing for months, which is due to the effective protection of silver nanoparticles against aggregation or release by the 'nano-tree' type polymer brushes.

3.2. Catalytic reduction of 4-nitrophenol

The kinetics of the prepared silver nano-composite particles to serve as catalyst for the reduction of 4-nitrophenol to 4-aminophenol has been studied by UV/vis spectroscopy. Fig. 11 shows the typical UV spectra for the reduction of 4-nitrophenol measured at different times. The rate constant can be obtained from the decrease of peak intensity at 400 nm with time. This peak is attributed to the 4-nitrophenate ions in the system, which appear immediately after addition of $NaBH_4$ to the system. After addition of silver nanocomposite particles, the peak at 400 nm decreases gradually with time and a new peak appears at 290 nm. This peak can be attributed to the product 4-aminophenol [49,50]. The conversion of the reduction reaction can be directly read off these curves inasmuch the ratio of the concentration c_t of the 4-nitrophenol

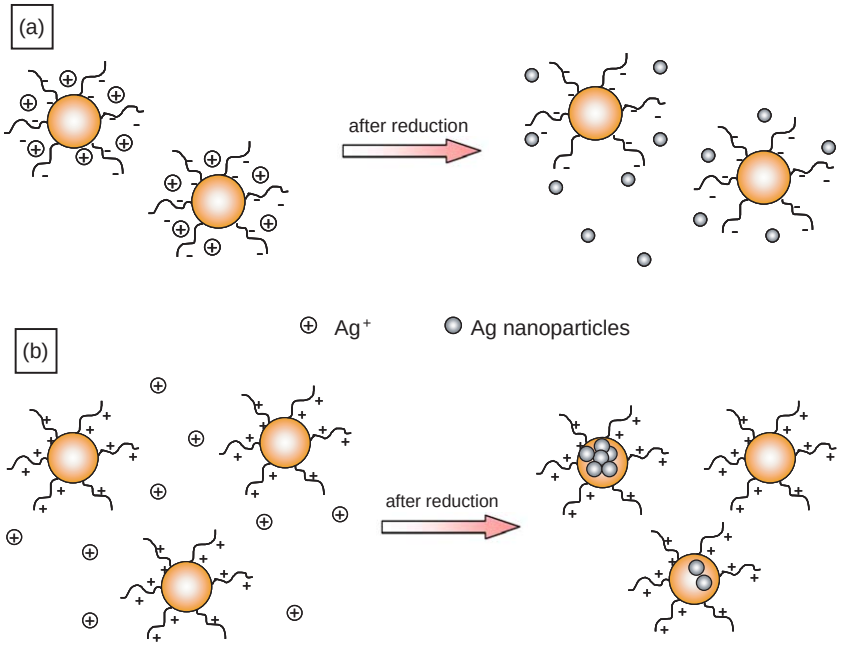

Fig. 7. Model for the preparation of Ag composite particles by using anionic (a) or cationic (b) spherical polyelectrolyte brushes as the template, respectively.

at time t to its value c_0 at $t=0$ is directly be given by the ratio of the respective absorbance A/A_0. Moreover, it is worth pointing out that two points can be observed in the UV spectra where all spectra intersect each other (see arrows in Fig. 11). This indicates that 4-aminophenol is the only product which is formed by the catalytic reduction reaction of 4-nitrophenol [22].

The concentration of sodium borohydride was adjusted to largely exceed the concentration of 4-nitrophenol. Therefore, reaction rates can be assumed to be independent of borohydride concentration. So in this case a first order rate kinetics with regard to the 4-nitrophenol concentrations could be used to evaluate the catalytic rate. Furthermore, the apparent rate constant k_{app} will certainly be proportional to the total surface S of the metal nanoparticles present in the system [22,28]

$$-\frac{dc_t}{dt} = k_{app}c_t = k_1 S c_t \quad (1)$$

where c_t is concentration of 4-nitrophenol at time t, k_1 is the rate constant normalized to S, the surface area of Ag nanoparticles normalized to the unit volume of the system.

As shown in Fig. 12, a linear relation between $\ln(c_t/c_0)$ versus time t has been obtained in all cases. Moreover, a delay time t_0 was found for the catalytic reductions, which were made under air. A similar behavior has been observed by other groups as well [3,8,42]. In order to investigate the reason for the delay time t_0 in the system, catalytic reductions have been also made after removal of oxygen. In this case, no delay time of t_0 has been observed as shown in Fig. 12. Furthermore, the kinetic curves measured after removal of oxygen at each silver concentration have the similar slope as that was made in the presence of oxygen, but just the starting point was shifted to the $t=0$ s. Thus, the delay time t_0 of the catalytic reductions is caused by the reduction of oxygen present in the system.

Obviously, the reduction of O_2 proceeds much faster than the one of the nitrophenol also present in the solution. The reduction reaction of nitrophenol only starts after all the oxygen in the system has been reacted. As the sodium borohydride is present in a large excess, its consummation by oxygen will not alter its concentration notably. It is also interesting to note that the delay time t_0 observed for present system is much longer than the other reported system [28]. This may be caused by a better solubility of oxygen in presence of the carrier system. This point is under further consideration now.

Fig. 13 shows the values of the apparent rate constant k_{app} measured with and without oxygen in the system as a function of concentration of Ag-composite particles and theoretical specific area of Ag particles, respectively. As shown in Fig. 13, the increase of the concentration of the silver nanoparticles in the system leads to rapid increase of the rate constant. Moreover, a strictly linear relation between k_{app} and the surface of the silver nanoparticles can be observed. This is obvious when we consider that the catalysis takes place on the surface of the metal nanoparticles. Therefore, the catalytic activity at given temperature must depend on the total surface area S of the metal nanoparticles immobilized per unit volume of the system. Moreover, the rate constant k_{app} follows the same linear function before and after removal of oxygen in the system, which indicates that the presence of oxygen will not influence the rate constant of the reduction reaction but just increase the t_0. Hence, the reduction reactions of O_2 and nitrophenol proceed strictly in sequence and do not interfere with each other.

In order to compare the specific turnover frequencies (TOF) of silver nanocomposites with other composite systems, the rate constant normalized to the surface area of Ag nanoparticles in the unit volume of the system has been

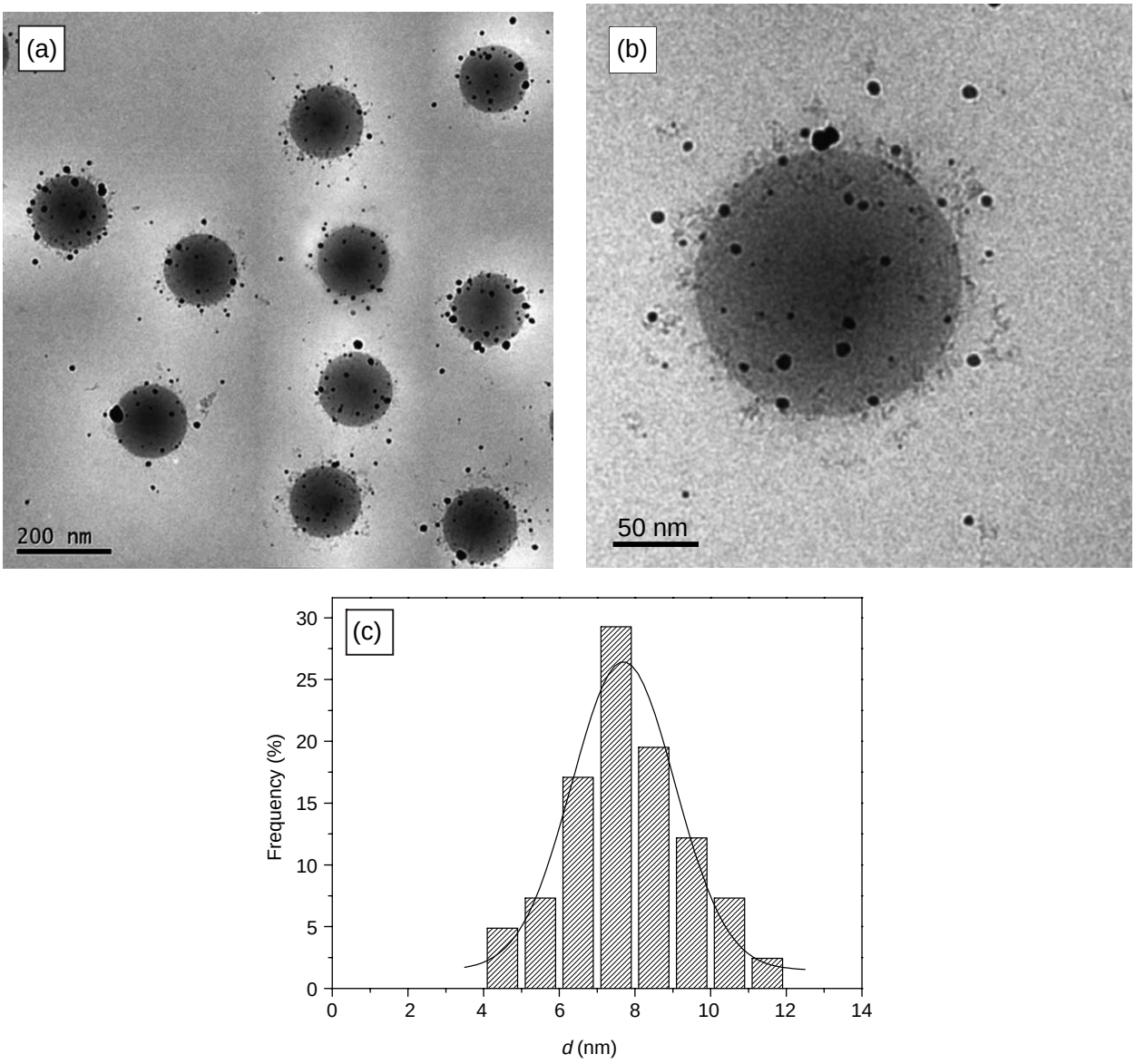

Fig. 8. Cryo-TEM images for PS–PEGMA–Ag composite particles (a) and an example for one silver composite particle (b), respectively, and the particle size distribution histogram of Ag particles evaluated from the cryo-TEM image (c). The solid line in (c) is the Gaussian fit of the data.

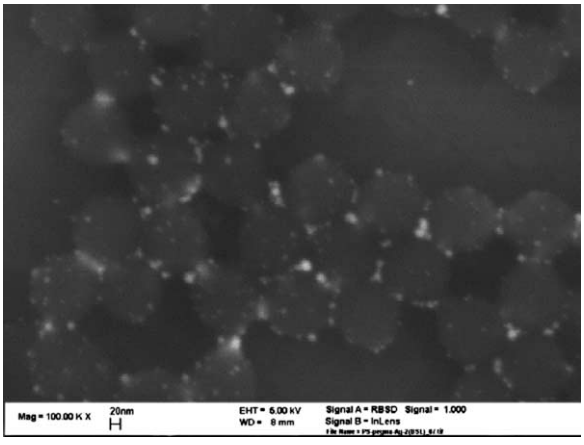

Fig. 9. FESEM image for PS–PEGMA–Ag composite particles with BSE mode.

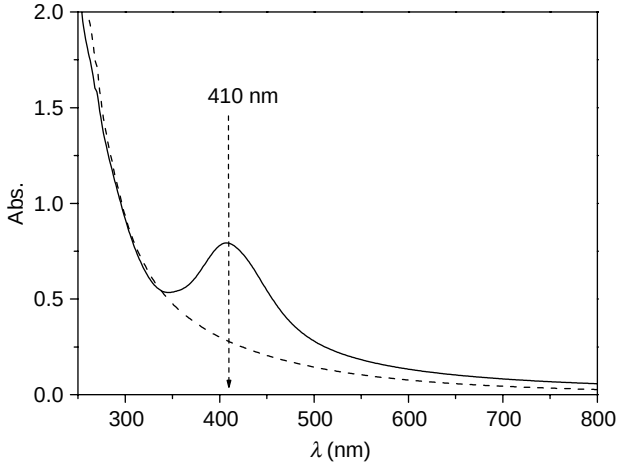

Fig. 10. UV/vis absorption spectra of the PS–PEGMA–$AgNO_3$ solution before (dash) and after (line) reduction.

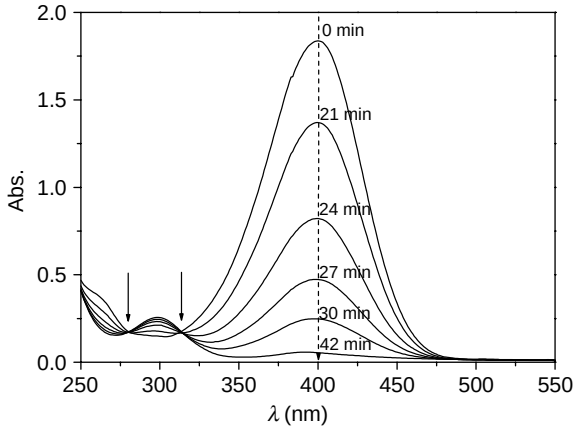

Fig. 11. UV/vis absorption spectra of solutions of 4-nitrophenol measured at different time t indicated in the graph. Arrows mark the points where all spectra intersect.

calculated. For the PS–PEGMA–Ag composite particles (Fig. 13(b)) we obtain $k_1 = 7.27 \times 10^{-2}\,s^{-1}\,m^{-2}\,l$. Table 3 gives the data of the catalytic activity of different metal nanoparticles, which have been reported in the reduction reaction of 4-nitrophenol with a large excess of $NaBH_4$ that is, under exactly the same conditions. Table 3 demonstrates that the silver nanoparticles in the PS–PEGMA–Ag composites exhibit the highest catalytic activity. This may due to the fact that the Ag particle prepared in present system is relatively smaller than the Ag particle prepared by the other carrier systems. Hence, the above result would indicate that smaller particles exhibit a considerably higher activity. Pt and Pd nanoparticles have also been used as the catalyst, which exhibit a higher catalytic activity than Ag nanoparticles. The reasons for these marked differences are not yet clear.

Fig. 14 shows the dependence of the rate of reaction on temperature. Again the pseudo-first order kinetics can be

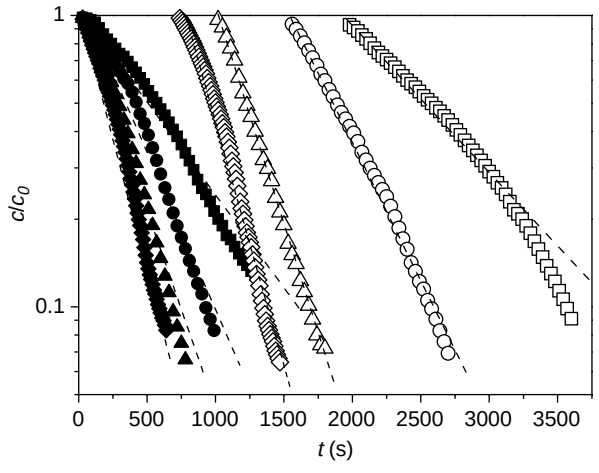

Fig. 12. Influence of Ag-composite particles (PS–PEGMA–Ag) concentration on the reduction of 4-nitrophenol. The concentration of the reactants was as follows: [4-nitrophenol] = 0.1 mmol/l, [$NaBH_4$] = 10 mmol/l, T = 20 °C. Parameter of the different curves is the concentration of composite particles in the solution. Quadrangles, 2.28 mg/l; circles, 3.42 mg/l; triangles, 4.56 mg/l; diamonds, 5.70 mg/l. Open symbols, measurements made under air; filled symbols, measurements made under N_2.

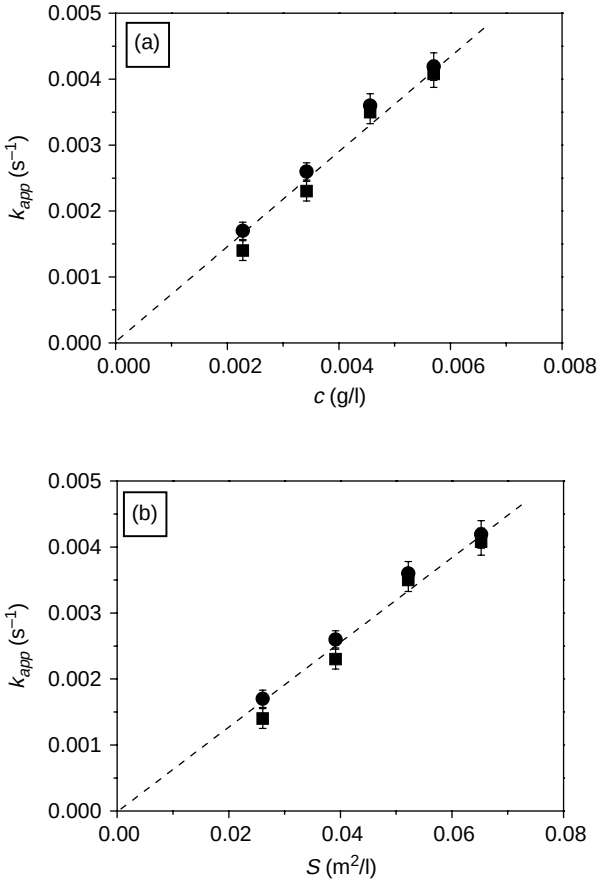

Fig. 13. Rate constant k_{app} as function of concentration of Ag-composite particles (a) and as function of the surface area S of Ag nanoparticles normalized to the unit volume of the system (b), respectively. Quadrangles, measured in presence of oxygen; circles, measured after removal of oxygen. T = 20 °C; [4-nitrophenol] = 0.1 mmol/l, [$NaBH_4$] = 10 mmol/l.

observed at all temperatures T. Moreover, the delay time t_0 is reduced with increasing temperature as expected from the analysis of other systems [22,28]. The rate constants $k_{app}(T)$ obtained from PS–PEGMA–Ag composite particles obtained from this analysis are shown in Fig. 15. Fig. 15 demonstrates that the rate constants k_{app} obtained at different temperatures

Table 3
Catalytic activity of the metal nanoparticles for the reduction reaction of 4-nitrophenol

Sample	Carrier system	Metal	D (nm)[a]	k_1 ($s^{-1}\,m^{-2}\,L$)[b]
PS–PEGMA–Ag	Highly branched polymer brush; this work	Ag	7.5 ± 2	7.27×10^{-2}
Ref. [22]	PS-NIPA core-shell particles	Ag	8.5 ± 1.5	5.02×10^{-2}
Ref. [42]	PVA	Ag	~25	3.78×10^{-7}
Ref. [28]	Cationic poly-electrolyte brush	Pt	2.1 ± 0.4	1.5
Ref. [28]	Cationic poly-electrolyte brush	Pd	2.2 ± 0.5	0.55

[a] D, diameter of the metal nanoparticles measured from cryo-TEM images.
[b] k_1, rate constant normalized to the surface of the particles in the system (Eq. (1)).

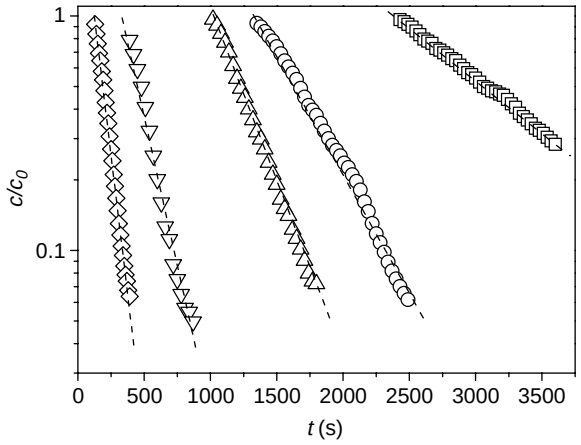

Fig. 14. Influence of temperature on the kinetic constant k_{app} measured with PS–PEGMA–Ag system. Parameter of the different curves is the temperature T. Quadrangles, 283 K; circles, 288 K; up triangles, 293 K; down triangles, 303 K; and diamonds, 313 K. The concentrations are follows: [PS–PEGMA–Ag] = 4.56×10^{-3} g/l, [4-nitrophenol] = 0.1 mmol/l, [$NaBH_4$] = 10 mmol/l.

follow the typical Arrhenius-type dependence on temperature. An activation energy $E_A = 62$ kJ/mol follows from this analysis. Moreover, the activation energy of the reciprocal delay time t_0 (64 kJ/mol) is practically the same as the one for the reduction of nitrophenol. Both reductions have obviously the same rate-determining step. This is accord with other studies for the catalysis of this reaction by metal nanoparticles [28]. The faster reduction of O_2 may then be related to its much higher diffusion coefficient. This problem is under further consideration by now.

4. Conclusion

A new polymer brush system with 'nano-tree' type morphology has been prepared by photo-emulsionpolymerization using functional macromonomer PEGMA as the monomer. These PS–PEGMA brushes can be used as 'nanoreactors' for generation and immobilization of Ag nanoparticles. Cryo-TEM and FESEM images show that Ag nanoparticles with diameter of $\sim 7.5 \pm 2$ nm are homogeneously embedded into the PS–PEGMA brushes. The PS–PEGMA–Ag composite particles can be used as catalyst for reduction reaction of 4-nitrophenol in the presence of sodium borohydride. Good colloidal stability of the carrier particles was observed under all conditions. Hence, the PS–PEGMA brushes may be used as robust carrier particles for immobilization of metal nanoparticles.

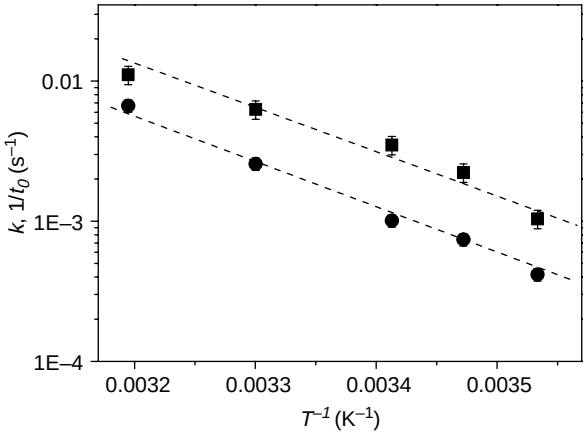

Fig. 15. Arrhenius plot of the reaction rate $k(T)$ measured in presence of PS–PEGMA–Ag (quadrangles) composite particles at different temperatures. The circles give the reciprocal delay time $1/t_0$. The concentrations of the reactants are: composite particles 4.56×10^{-3} g/l, [4-nitrophenol] = 0.1 mmol/l, [$NaBH_4$] = 10 mmol/l.

Acknowledgements

The authors thank the Deutsche Forschungsgemeinschaft, SFB 481, Bayreuth, the BASF-AG, and Fonds der Chemischen Industrie for financial support.

References

[1] Burda C, Chen X, Narayanan R, El-Sayed MA. Chem Rev 2005;105(4):1025–102.
[2] Jiang ZJ, Liu CY, Sun LW. J Phys Chem B 2005;109(5):1730–5.
[3] Praharaj S, Nath S, Ghosh S, Kundu S, Pal T. Langmuir 2004;20(23):9889–92.
[4] Narayanan R, El-Sayed MA. J Phys Chem B 2005;109(26):12663–76.
[5] Campbell CT, Parker SC, Starr DE. Science 2002;298(5594):811–4.
[6] Frederix F, Friedt J, Choi K, Laureyn W, Campitelli A, Mondelaers D, et al. Anal Chem 2003;75(24):6894–900.
[7] Scott RWJ, Wilson OM, Crooks RM. J Phys Chem B 2005;109(2):692–704.
[8] Esumi K, Isono R, Yoshimura T. Langmuir 2004;20(1):237–43.
[9] Liu ZL, Wang XD, Wu HY, Li CX. J Colloid Interface Sci 2005;287(2):604–11.
[10] Chen CW, Chen MQ, Serizawa T, Akashi M. Adv Mater 1998;10(14):1122–6.
[11] Kim JW, Lee JE, Ryu JH, Lee JS, Kim SJ, Han SH, et al. J Polym Sci, Part A: Polym Chem 2004;42(10):2551–7.
[12] Chen CW, Serizawa T, Akashi M. Langmuir 1999;15(23):7998–8006.
[13] Sun Q, Deng Y. Langmuir 2005;21(13):5812–6.
[14] Carotenuto G. Appl Organometal Chem 2001;15(5):344–51.
[15] Vincent T, Guibal E. Langmuir 2003;19(20):8475–83.
[16] Biffis A, Orlandi N, Corain B. Adv Mater 2003;15(18):1551–5.
[17] Biffis A, Sperotto E. Langmuir 2003;19(22):9548–50.
[18] Pich A, Hain J, Lu Y, Boyko V, Prots Y, Adler HJ. Macromolecules 2005;38(15):6610–9.
[19] Zhang J, Xu S, Kumacheva E. J Am Chem Soc 2004;126(25):7908–14.
[20] Zhang J, Xu S, Kumacheva E. Adv Mater 2005;17(19):2336–40.
[21] Lu Y, Mei Y, Drechsler M, Ballauff M. Angew Chem, Int Ed Engl 2006;45(5):813–6.
[22] Lu Y, Mei Y, Drechsler M, Ballauff M. J Phys Chem B 2006;110(9):3930–7.
[23] Suzuki D, Kawaguchi H. Langmuir 2005;21(18):8175–9.
[24] Mbhele ZH, Salemane MG, Van Sittert CGCE, Nedeljkovic JM, Djolovic V, Luyt AS. Chem Mater 2003;15(26):5019–24.
[25] Scott RW, Wilson OM, Oh SK, Kenik EA, Crooks RM. J Am Chem Soc 2004;126(47):15583–91.
[26] Oh SK, Niu Y, Crooks RM. Langmuir 2005;21(22):10209–13.
[27] Sharma G, Ballauff M. Macromol Rapid Commun 2004;25(4):547–52.
[28] Mei Y, Sharma G, Lu Y, Drechsler M, Ballauff M, Irrgang T, et al. Langmuir 2005;21(26):12229–34.
[29] Das B, Guo X, Ballauff M. Prog Colloid Polym Sci 2002;121:34–8.
[30] Meier LP, Sgekdeb RA, Caseru WR, Suter UW. Macromolecules 1994;27(6):1637–42.
[31] Rühe J. Macromol Symp 1997;126:215–22.

[32] Ballauff M. Macromol Chem Phys 2003;204(2):220–34.
[33] Nomura E, Ito K, Kajiwara A, Kamachi M. Macromolecules 1997;30(10): 2811–7.
[34] Maniruzzaman M, Kawaguchi S, Ito K. Macromolecules 2000;33(5): 1583–92.
[35] Wu C, Akashi M, Cheri MQ. Macromolecules 1997;30(7):2187–9.
[36] Pich A, Lu Y, Alder HJ. Colloid Polym Sci 2003;281(10):907–15.
[37] Hu Z, Lu X, Gao J, Wang C. Adv Mater 2000;12(16):1173–6.
[38] Guo X, Weiss A, Ballauff M. Macromolecules 1999;32(19):6043–6.
[39] Nizri G, Magdassi S, Schmidt J, Talmon Y. Langmuir 2004;20(11): 4380–5.
[40] Li Z, Kesselman E, Talmon Y, Hillmyer MA, Lodge TP. Science 2004; 306(5693):98–101.
[41] Wittemann A, Drechsler M, Talmon Y, Ballauff M. J Am Chem Soc 2005; 127(27):9688–9.
[42] Pradhan N, Pal A, Pal T. Colloids Surf A 2002;196(2/3):247–57.
[43] Guo X, Ballauff M. Langmuir 2000;16(23):8719–26.
[44] Van Hyning D, Zukoshi C. Langmuir 1998;14(24):7034–46.
[45] Behrens S, Wu J, Habicht W, Unger E. Chem Mater 2004;16(16): 3085–90.
[46] Teranish T, Kiyokawa I, Miyake M. Adv Mater 1998;10(8): 596–9.
[47] Porel S, Singh S, Harsha SS, Rao DN, Radhakrishnan TP. Chem Mater 2005;17(1):9–12.
[48] Patakfalvi R, Viranyi Z, Dekany I. Colloid Polym Sci 2004;283(3): 299–305.
[49] Antipov AA, Sukhorukov GB, Fedutik YA, Hartmann J, Giersig M, Moehwald H. Langmuir 2002;18(17):6687–93.
[50] Ghosh SK, Mandal M, Kundu S, Pal T. Appl Catal A 2004;268(1–2): 61–6.